To appear in the *Proceedings of the International Conference on Lasers '98*

RECENT ADVANCES IN IMAGING AND SPECTROSCOPY WITH T-RAYS

Daniel Mittleman, Ramesh Neelamani, Maya Gupta,[*] and Richard Baraniuk
Electrical and Computer Engineering Dept., MS-366
Rice University
6100 Main St.
Houston TX 77005

Martin C. Nuss
Bell Laboratories, Lucent Technologies, Holmdel, NJ

Abstract

Recent work in terahertz "T-Ray" imaging is reported. With the ongoing development of commercially viable THz-TDS imaging system, optimal signal processing strategies for the THz waveforms must be developed. Algorithms based on wavelet decomposition of the time and frequency-localized signals offer a number of advantages. Examples of denoising, deconvolution, and other waveform analysis tools are described.

Introduction

We have recently described a new imaging modality, based on terahertz time-domain spectroscopy.[1,2] Here, we discuss the extension of T-ray imaging to 3-dimensional tomographic imaging, by analyzing the temporal structure of THz waveforms returned from objects in a reflection geometry. The return time of reflected pulses directly correlates with the location of the dielectric interfaces along the propagation direction of the beam. Because the arrival time of the THz waveforms can be determined with an accuracy of a few femtoseconds, i.e., much less than the pulse duration, the positions of reflecting surfaces within the object under study can be determined with an accuracy of a few microns, when successive reflections are well separated in time.[3] In contrast to the two-dimensional T-ray transmission images published earlier, it is now possible to obtain full volume images of many objects in the terahertz frequency range.

The experimental setup is described in detail in reference 2. The beam of THz pulses is incident on the sample at nearly normal incidence, and comes to a focus at the sample surface. The beam reflected from the object is re-collimated, then captured by a pick-off mirror, which directs it to the receiver antenna. The generation, detection and real-time processing of the THz waveforms are similar to what is described in the original transmission experiments.[1]

For an object with multiple reflecting internal surfaces, the reflected waveform consists of a series of replicas of the input pulse of varying magnitude, polarity, and temporal distortion. This is illustrated using the example of a ball-point pen. The input and reflected THz waveforms from a single point on the pen are shown in figure 1. The upper waveform (figure 1a) is obtained by replacing the object with a mirror, and thus represents the pulse incident on the sample. The small oscillations which follow the main pulse in this waveform are a result of residual water vapor in the beam path,[4] as well as electrical impedance mismatch effects in the antennas. The second curve (figure 1b), a representative reflected waveform, consists of a series of replicas of the input waveform. These correspond to reflections from the dielectric interfaces of the pen, either from air to plastic, or plastic to air. The polarity and magnitude of each reflection are given by the reflection coefficient at each interface, and are related to the size and sign of the corresponding index step. In this example, the temporal waveforms hardly change shape while traversing the object because the plastic material has little absorption and dispersion. In a more general situation, reflected waveforms may be significantly altered in shape.

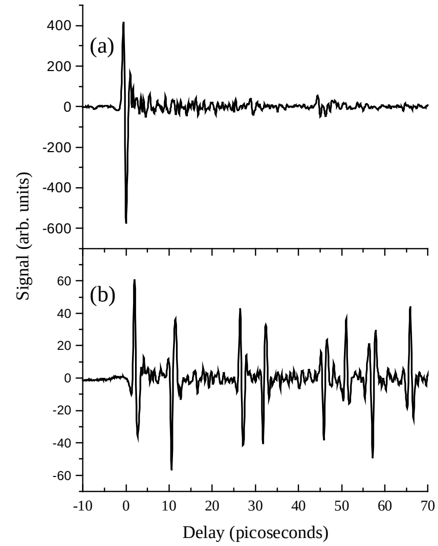

Figure 1 Terahertz waveforms (a) incident on, and (b) reflected from a ball-point pen.

Deconvolution

In order to accurately extract information from a measured waveform, it is necessary to distinguish between those features which result from the interaction of the radiation with the sample under study and those which are intrinsic to the THz system, i.e., the instrument response function. An illustrative example of this is found in the application of terahertz time-domain spectroscopy for gas sensing.[5,6] Figure 2 depicts sample gas sensing data. It shows the THz waveform transmitted through a ~30 cm gas cell, both (a) without and (b) with a sample gas (in this case, HCl) present. Curve (b) (signal) displays the distortions imposed on the waveform, in the time domain, by the absorption in the gas. Note that the 'ringing' which constitutes the signature of the gas closely resembles the features which follow the main pulse in curve (a) (reference). These features (largest ones indicated by arrows) are a result of either electrical or optical reflections, due to impedance mismatches in the emitter antennas, multiple reflections in the cell windows, or similar effects. These are characteristic of the THz system, and not of the action of the gas, and they therefore appear identically in both waveforms. This close resemblance between features of the reference waveform and the signatures of the gas can limit the effectiveness of any estimation algorithm designed to extract quantitative gas concentrations. Evidently, a robust means for deconvolving this known system response function, including both the initial peak *and* the subsidiary reflections, will improve the performance of the gas identification system.

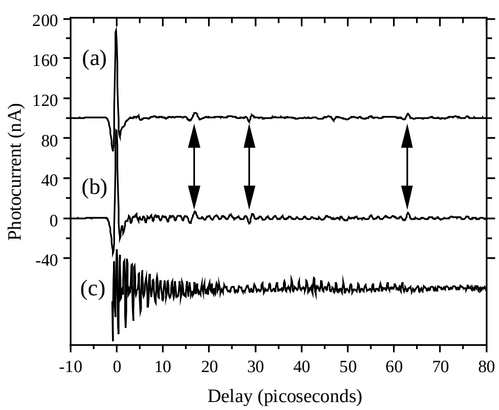

Figure 2 (a) reference waveform transmitted through gas cell. (b) waveform transmitted through cell containing ~13 kPa of HCl vapor. (c) signature of the gas, deconvolved from (b) as outlined in the text.

One obvious solution is to perform a *deconvolution* of these features by means of a ratio in the Fourier domain. However, it is desirable to design a linear filter which simultaneously deconvolves the unwanted impulse response and discriminates against measurement noise. A Wiener deconvolution filter balances deconvolution and noise filtering. The transfer function of such a filter is given by

$$G(f) = \frac{I^*(f)P(f)}{|I(f)|^2\, P(f) + \sigma_n^2} \tag{1}$$

where $I(f)$ is the spectrum of the impulse response, P(f) is the power spectrum of the input, and σ_n^2 is the variance of the measurement noise, assumed here to be white noise.[7] The power spectrum of the input is not directly measured here, but a reasonable approximation can be obtained by simply inserting the known high-frequency cutoff of the spectrum, ~2.1 THz in this example. The result of this simultaneous denoising and deconvolution is shown in Figure 2c. Here, all of the features in the time-domain waveform which appear in the reference have been removed, leaving only the oscillatory features induced by the gas.

<u>Wavelet Processing of THz Waveforms</u>

Since THz pulses are localized in both time and frequency, they are naturally suited to signal processing methods based on *wavelets*. This is particularly true for tomographic imaging data, such as shown in Figure 1. The wavelet transform performs a ‘local Fourier analysis’ by analyzing and representing signals in terms of shifted and dilated versions of time-localized, oscillating functions.[8] Since the elements of a wavelet basis can be designed to closely resemble the underlying waveforms in the THz system, wavelet-based signal processing algorithms will outperform more traditional techniques. Indeed, it has been shown that noise removal, compression, and signal recovery methods based on wavelet coefficient shrinkage or wavelet series truncation enjoy excellent asymptotic performance and moreover, do not introduce excessive artifacts in the signal reconstruction.[9] Thus wavelets appear to be a natural tool for addressing the processing challenges presented by the THz-TDS system, including tomographic image reconstruction.

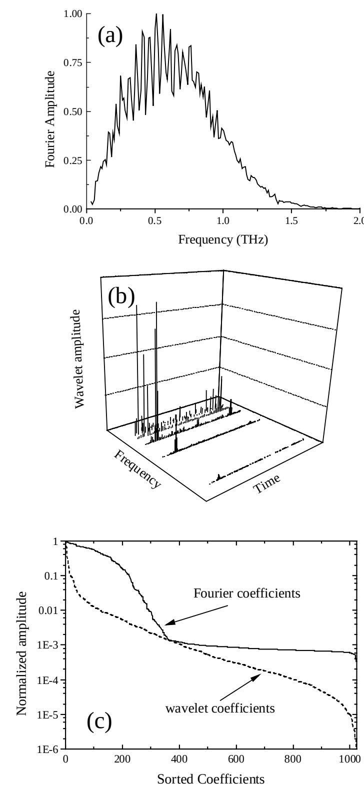

Figure 3 (a) Fourier representation of the waveform from Figure 4a. (b) Wavelet representation of the same waveform. (c) The two sets of 1024 coefficients, sorted in descending order. There are far fewer wavelet coefficients of significant amplitude.

Measurement noise is an issue which will inevitably limit the performance of the sensing system, particularly as the speed of waveform acquisition is increased. Removing noise from a measured waveform prior to processing will be an important aspect of any pre-processing procedure. Wavelet-based denoising will be far superior to the more familiar Fourier-based techniques.[9,11] particularly when the raw data resembles the waveforms of Figure 4. Because the elements of a wavelet basis can be tailored to closely resemble these THz-TDS signals, fewer coefficients are required to represent the signals in a wavelet basis than in a Fourier expansion. This is illustrated in Figure 3, using the waveform of Figure 4a as an example. Here, Figures 3a and 3b depict the representations of this data in the Fourier and wavelet bases, respectively. Because the wavelet transformation is a mixed time-frequency representation, the wavelet decomposition of a temporal waveform is displayed in a two-dimensional format, as shown. This display (b) shows that the wavelet representation requires a small number of coefficients of significant amplitude, mostly localized along the time axis at the two positions where the waveform is large. In (c), the

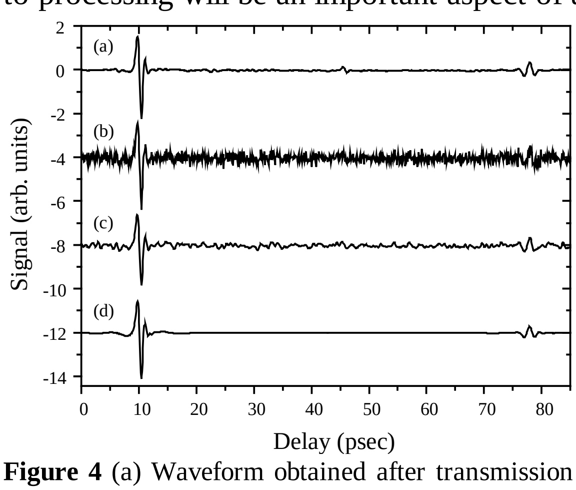

Figure 4 (a) Waveform obtained after transmission through acetonitrile vapor. The small echo at ~78 psec delay is the first rephasing of the rotational manifold [10], and thus represents the signature of the gas. (b) Same waveform, with ~10% white Gaussian noise added numerically. (c) Curve (b) denoised using a Butterworth filter. (d) Curve (b) denoised using a wavelet filter with soft thresholding.

1024 coefficients in these two expansions are sorted in descending order, and displayed on a logarithmic scale. The Fourier coefficients decay more slowly, confirming that more large coefficients are required for an accurate representation of the signal. Also, the noise floor at ~10^{-3} of the peak signal is evident, where the curve exhibits a ‘knee’ followed by a noise-limited plateau. A simple Fourier-based denoising would consist of truncation of these coefficients at this point, thus reducing the number of non-zero coefficients from 1024 to ~360. The wavelet coefficients decay far more rapidly, thus permitting a truncation much sooner. This enables a far more efficient denoising strategy, as well as substantial signal compression. Figure 4 shows a comparison of denoising of a THz waveform using these two methods. Here, a THz waveform is artificially supplemented with white Gaussian noise (Figure 4b), and subsequently processed using both a parabolic Fourier filter (Figure 4c) and a soft threshold in the wavelet domain (Figure 4d). The wavelet denoising is evidently far superior for this type of noise. The development of a wavelet-based denoising strategy for 1/f noise, of the type expected in these measurements, is a topic of current research.

The waveform reflected from the pen (Figure 1b) can be used to illustrate an additional capability of wavelet processing. Evidently, each reflected pulse in this pulse train contains information about each of the layers through which it passed, as well as the interface off of which it reflected. By analyzing the first pulse in the sequence, it should be possible to extract spectroscopic information about the first interface encountered, including both the frequency-dependent absorption and refractive index. This information could then be used, in combination with the second pulse in the sequence, to determine these parameters for the second layer. This iterative procedure should permit full spectroscopic analysis in combination with tomographic imaging.

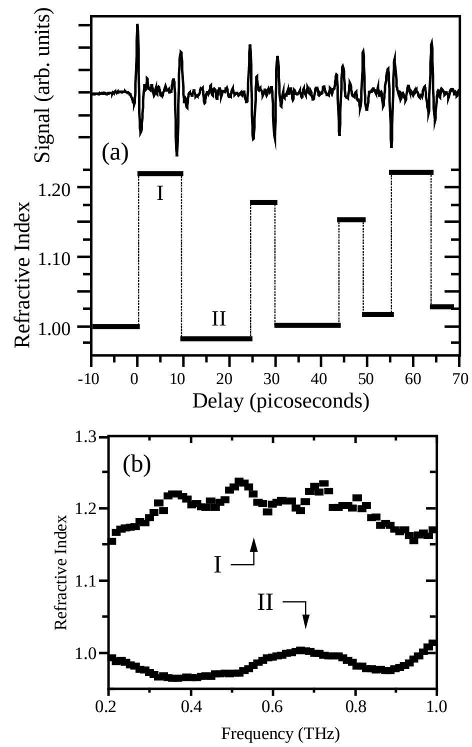

Figure 5 (a) The average refractive index profile of the ball-point pen, extracted from the reflected waveform, which is reproduced here for comparison. (b) The frequency-dependence of the refractive indices in the two regions (one of plastic, and one of air) labeled with Roman numerals in (a).

Because the wavelets effectively permit a local analysis of each reflected pulse in the pulse train, they are a natural tool for an analysis of this type. Figure 5 shows early results of such an analysis. In Figure 5a, the average refractive index profile is extracted, as a function of depth into the material. Evidently, the alternating air-plastic-air structure is well reproduced, although the small amplitude noise mentioned above limits the accuracy of this procedure. Figure 5b shows the results of the spectroscopic analysis for two of the regions identified in the upper figure. Again, the noise limits the accuracy of the technique. Implementation of the aforementioned wavelet-based denoising prior to this spectroscopic analysis should improve these results.

* Present address: Electrical Engineering Department, Stanford University

[1] B. B. Hu and M. C. Nuss, *Opt. Lett.*, **20**, 1716 (1995).
[2] D. M. Mittleman, R. H. Jacobsen, and M. C. Nuss, *IEEE J. Selected Topics in Quant. Elec.,* **2**, 679 (1996).
[3] D. M. Mittleman, S. Hunsche, L. Boivin, and M. C. Nuss, *Opt. Lett.*, **22**, 904 (1997).
[4] M. van Exter, C. Fattinger, and D. Grischkowsky, *Opt. Lett.*, **14**, 1128 (1989).

[5] R. H. Jacobsen, D. M. Mittleman, and M. C. Nuss, *Opt. Lett.,* **21**, 2011 (1996).
[6] D. M. Mittleman, R. H. Jacobsen, R. Neelamani, R. G. Baraniuk, and M. C. Nuss, *App. Phys. B*, **67**, 379 (1998).
[7] K. R. Castleman, *Digital Image Processing* (Prentice-Hall, Englewood Cliffs, NJ, 1996).
[8] I. Daubechies, *Ten Lectures on Wavelets* (Society for Industrial and Applied Mathematics, Philadelphia, 1992).
[9] D. Donoho, *IEEE Trans. Info. Theory*, **41**, 613 (1995).
[10] H. Harde, S. R. Keiding, and D. Grischkowsky, *Phys. Rev. Lett.*, **66**, 1834 (1991).
[11] S. Ghael, A. M. Sayeed, and R. G. Baraniuk, *Proc. SPIE*, San Diego, July 1997.